Numerical Modeling of Time-Mean Flow at Isolated Seamounts

A. Beckmann

Alfred-Wegener-Institute for Polar and Marine Research, Bremerhaven, F.R.Germany

Abstract. A numerical σ-coordinate ocean circulation model is used to investigate the strength and spatial structure of rectified flow at the flanks of a tall and steep isolated seamount. This study is closely related to and motivated by the studies of flow around Fieberling Guyot in the northeast Pacific; however, an idealized form of the topography, both smooth and with irregularities, is prescribed. A series of experiments with varying resolution and geometrical/environmental parameters is analyzed for mean flow generation. A regime is found where the presence of the rectified flow influences the wave amplification. The efficiency of the rectification mechanism is quantified for a wide range in parameter space. The along-isobath flow is generally bottom intensified, with its maximum very close to the seamount's summit. Finally, the model results are briefly compared to simple theoretical concepts for parametrization of flow-topography interaction effects.

Introduction

Isolated submarine topography is known to be the source of mesoscale variability in the ocean and therefore of great importance for the local and regional environment. Time-dependent forcing will generate transient density perturbations and flow intensifications at the seamount which propagate in form of "seamount trapped waves" clockwise (on the northern hemisphere) along closed depth contours. In particular, periodic forcing is capable of producing a strong wave response by resonant amplification. In addition to these time-variable phenomena, steady solutions of flow around isolated seamounts exist: both are due to the steady part of the forcing (uniform far field "climatological" flow) and to the nonlinear rectification processes at the seamount itself.

There is a large body of literature on the influence of such isolated topography on the circulation in the ocean and atmosphere. Hogg (1980) gives a comprehensive overview of early theoretical studies. Recent observations (Eriksen, 1991; Brink, 1995), advanced analytical treatment of quasigeostrophic flow past obstacles (Fennel and Schmidt, 1991), and laboratory realizations of stratified seamount trapped waves (Codiga, 1993) are evidence for continued and even increased interest.

The purpose of numerical modeling is to extend these prior studies to more realistic (fully non-linear) regimes. Progress with primitive equation modeling of steep and tall topography was made only very recently (Chapman and Haidvogel, 1992, 1993; Haidvogel et al., 1993). In idealized configurations smooth, symmetric seamounts in a fluid with linear or exponential stratification and forced by steady or diurnally varying barotropic ambient flow are studied.

In an attempt to prepare us for models featuring real bathymetry, some of the following questions will be addressed:

— the role of resolution;

— the role of individual processes (nonlinearity, stratification); and

— the role of topographic scale changes and irregularities.

Finally, the implications for parametrization of the mean flow rectification will be considered briefly.

The Spatial Structure of Trapped Flow at Seamounts

Seamount Trapped Waves

Theoretically, an infinite set of trapped waves exists at isolated seamounts, at discrete sub-inertial frequencies and azimuthal wavenumbers (Brink, 1989). In practice, only the gravest modes have been observed in reality and found in numerical models. The linear waves have one up- and one down-welling lobe; most of the flow crosses the seamount's summit and returns at the flanks (see Brink, 1989). These waves were found to occur broadly in parameter space, both as a function of stratification and forcing frequency (Haidvogel et al., 1993). Trapped waves of near-diurnal frequency are of particular interest, because the forcing at the tidal periods K_1 and O_1 are dominant in many parts of the open ocean.

In previous studies on the influence of stratification, the Burger number

$$S^* = \frac{NH}{fR} \tag{1a}$$

has been used as a combined measure of stratification and rotation, where N is a vertical average Brunt-Väisälä frequency, H the maximum water depth, f the Coriolis parameter and R the horizontal scale of the seamount.

Acknowledging that seamount trapped waves are in most cases limited to the upper flanks of the topography, the choice of N and H as representative of the whole water column seems inappropriate. Consequently, for this study the Burger number was defined as the first internal Rossby radius of deformation r_D at the seamount's summit relative to the seamount radius R,

$$S = \frac{r_D}{R}, \qquad (1b)$$

thus representing an integral measure of the stratification at the location of the maximum of the seamount trapped wave. We will look at values of S of order 1. For comparison, the Burger number range in the Haidvogel et al. (1993) study is $S = 0$ to 0.2.

Time-Mean Flow

The time-mean flow at isolated seamounts can reach O(10 cm s^{-1}) (e.g., Brink, 1995 at Fieberling Guyot), about 50% of the observed wave amplitude. This mean flow is thought to be the result of non-linear momentum and density advection of the seamount trapped wave. The strength of the mean circulation depends first and foremost on the amplitude of the generating wave, which in turn is a function of the environmental parameters (like stratification, rotation, forcing). The rectification efficiency (defined as mean flow amplitude relative to wave amplitude) found in numerical models (see Haidvogel et al., 1993) is a few tens of %, even at maximum resonance.

The dynamical balance for the dominant azimuthal component of the mean flow consists of radially inward (upslope) directed horizontal eddy fluxes of momentum, compensated by radially outward (downslope) mean advection. Correspondingly, the net inward mean transport of heat is balanced by outward eddy heat fluxes. This leads to a cap of dense water on top of the seamounts.

The time-mean secondary circulation is directed clockwise around the mean flow, featuring downwelling in the center of the vortex.

Although substantial mean flows were found in previous idealized models of flow around seamounts, effects of the presence of the mean flow on the wave propagation and/or resonance were not observed: the rectified flow seemed to be linearly superimposed on the propagating wave.

A Model of Flow at Fieberling Guyot

Preliminary results are available from a high resolution simulation of the response to tidal forcing of the stratified, non-linear ocean at Fieberling Guyot (Beckmann and Haidvogel, 1994). Their numerical model is a variant of the semi-spectral primitive equation model SPEM (Haidvogel et al., 1991) with a terrain-following vertical ("sigma") coordinate and a spectral approach in the vertical.

The experimental configuration is very similar to the idealized studies of Haidvogel et al. (1993): the computational domain is a periodic f-plane channel. The horizontal grid is "stretched," focussing on the seamount; the grid spacing is less than 1000 m in the seamount vicinity. The topography was derived from a high resolution data set and linearly interpolated to the numerical grid. No further smoothing of the bottom relief was applied.

The model is initialized with an exponential background stratification (fitted to measurements in the vicinity of Fieberling Guyot) and driven by a diurnal period barotropic current. The 1 cm s^{-1} amplitude and north-south orientation of the forcing are idealizations made from observations (Brink, 1995). A weak biharmonic lateral viscosity/diffusivity of 10^7 m^4 s^{-1}, linear bottom friction of $3 \cdot 10^{-4}$ m s^{-1} and a bottom-intensified vertical viscosity are used.

The model is spun up for 25 days before the model fields are averaged over one wave period. Both the instantaneous and the time-mean flow fields show several of the observed characteristics: A trapped wave of 12.6 cm s^{-1} amplitude is generated, setting up an anticyclonic time-mean flow at the upper flanks of the seamount of 6.2 cm s^{-1} (rectification efficiency of about 50%). The depth dependent vertical viscosity was found to improve the vertical structure of the simulated mean flow. Other characteristic properties of the model results compare less favorably with the observations. The vertical phase gradients and the secondary circulation of the mean flow are not yet reproduced realistically. More detailed analyses of these and future model results will be published in a forthcoming paper.

A comparison run with a smooth Gaussian fit to the topography give slightly smaller values of wave and mean flow. This is a first indication that topographic irregularities can alter the wave and mean flow response; it is unclear, though, whether this happens for purely geometric reasons (large scale asymmetries; locally steeper slopes) or by the presence of an additional rectification mechanism (form stress, see Haidvogel and Brink, 1986; Holloway et al., 1989) on these smaller scales.

This simulation with realistic topography represents a major step beyond previous idealized studies and it is far from straightforward to interpret the results. The runs differ in various respects: The forcing amplitude is larger by a factor of 5, and we expect both larger absolute values of wave-related currents and a more intense mean flow. At the same time, the higher horizontal resolution (by a factor of 8) and the correspondingly smaller values of diffusivity/viscosity (by a factor of 2/100) might also increase the response of the waves. The more realistic (i.e., generally stronger) stratification will have an

influence on the vertical decay scale of the trapped response.

The real geometry is characterized by a smaller radius and steeper flanks than used in previous studies; their effects on wave amplification and mean flow generation has not been investigated. The geometric and environmental situation yields a Burger number regime that has never before been explored and simple extrapolations into this parameter range are not very well justified. Finally, the asymmetries of the real seamount and the background bottom roughness on various scales may contribute in various ways: Both a net damping effect on the waves and an enhancement of the mean flow via the form stress mechanism seem plausible.

Parameter Studies

In this section we try to answer the question "Which factors contribute in what way to the generation of mean flow at real seamounts?" In order to investigate these issues, a series of some 60 experiments were carried out, exploring the sensitivity to various environmental and geometrical seamount properties.

The Model Configuration

The model used here is the latest version of the terrain-following sigma coordinate model SPEM (Haidvogel et al. 1991), which is formulated with finite differences on a staggered vertical grid. The model employs a fourth order algorithm (McCalpin, 1994) to reduce the spurious flow generated by the truncation errors of the pressure gradient terms. Models of this type have now been repeatedly and successfully applied in configurations with large variations in depth (Chapman and Haidvogel, 1992, 1993; Haidvogel et al., 1993; Beckmann and Haidvogel, 1994).

The basic shape of the seamount was chosen to accommodate several features of real seamounts, which are found to be tall and steep, and relatively flat on top. In particular, the seamount was not assumed Gaussian, but rather of a tanh-shape. As a consequence, the diameter and the slope can be prescribed separately. The functional form is

$$H = H_o + \Delta H \tanh((r - R_o)/R) \qquad (2)$$

with

$$H_o = 2500 \text{ m}$$
$$\Delta H = 2000 \text{ m}$$
$$R_o = 20000 \text{ m}$$
$$R = 8000 \text{ m}$$

The resulting maximum slope $(\nabla H)|_{max} = 25$ % is close to observed gradients.

This seamount was placed in the center of the periodic channel domain of 256 × 256 km. To account for the expected bottom trapped nature of both the seamount trapped wave and the mean flow, the vertical grid is stretched quadratically towards the bottom, as depicted in Figure 1. In comparison to an equidistant discretization this improves the resolution at the lower boundary of the model dramatically: the minimum grid spacing is 3.5 m at the top of the seamount and 35 m in the deep ocean; the maximum grid spacing just below the surface varies between 80 and 800 m. The horizontal resolution was chosen to be 2 km uniformly across the model domain; the Coriolis parameter of $f_o = 1.03 \cdot 10^{-4}$ s^{-1} corresponds to 45°N.

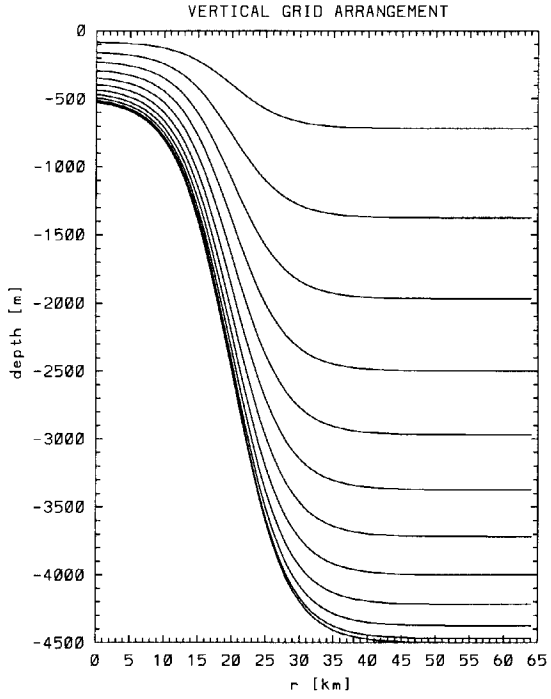

Figure 1. Coordinate lines form the quadratically stretched vertical grid as a function of radial distance from the seamount's center.

An exponential initial stratification of realistic strength was prescribed as

$$\rho = 28.0 - 2.5 \cdot e^{-(z/1000\text{ m})} \qquad (3)$$

with a corresponding Rossby radius of 9 km over the seamount's summit and 36 km in deep water, typical for mid-latitudes in the North Pacific. The Burger number for this experiment is

$$S = \frac{r_D}{R} = 0.5 \qquad (4)$$

(for comparison, $S^* = 11$).

Similar to previous idealized studies, the model is forced with diurnal barotropic tidal forcing of the form

$$u_f = U_o \tanh(t/3T)\sin(2\pi t/T) \quad (5)$$

with $U_o = 1$ cm s^{-1} and $T = 1$ day.

The viscous and diffusive terms are of particular importance for the amplification and rectification process. A standard linear bottom friction of $r_b = 3 \cdot 10^{-4}$ m s^{-1} was chosen in addition to a weak background biharmonic lateral viscosity/diffusivity $\nu_{uv} = \nu_\rho = 10$ [illegible] m^4 s^{-1}. The experiments were run for 20 days with a time step of 43.2 s; the last day was averaged to obtain the time-mean fields.

The Central Experiment

The central experiment serves as the standard solution and is used to illustrate the spatial structure of the wave and the mean flow. Table 1 lists the maximum point-wise velocities for the central experiment and, for comparison, identical experiments with linearized dynamics or homogeneous fluid.

Table 1. Maximum point-wise velocities for the central experiment and two additional runs with different physics.

	central reference	linearized dynamics	homogeneous fluid
total			
$\vec{v}_{WAVE}$	55.61	28.87	-
$\vec{v}_{MEAN}$	31.37	0.35	-
ratio	56%	1.2%	-
barotropic			
$\vec{v}_{WAVE}$	4.73	4.67	14.61
$\vec{v}_{MEAN}$	1.68	0.06	0.90
ratio	36%	1.2%	6%

The wave and mean flow amplitudes are quite large, and although wave amplifications of O(50) have been reported before, a mean flow of this strength has not been found in previous numerical models. It is interesting to note that the barotropic part is only a small fraction (9 and 6 %) of the wave and mean flow fields, respectively.

Figure 2 shows a snapshot of the density perturbation at various depths. At the upper flanks of the seamount (600 and 700 m) the first azimuthal mode seamount trapped wave is clearly visible. Right above the seamount's summit the additional cap of denser water dominates the density perturbation. The highly bottom trapped nature of both the wave and the mean flow becomes clear at the 400 m level, where only a weak indication of the wave is visible.

The mean flow in Figure 3 shows a similar structure as found in Haidvogel et al. (1993), but with much more pronounced bottom trapping. The mean flow is along isobaths for the most part, but even the secondary circulation in the radial-vertical plane is quite substantial: a radially outward current of up to 7 cm s^{-1} at the bottom returns in a thin layer of fluid above. The circulation is closed by downwelling in the center of the seamount of up to 100 m/day and a somewhat weaker upwelling motion above the upper flanks.

Unlike in the studies by Haidvogel et al. (1993), where the wave amplitude differed only insignificantly between linearized and non-linear dynamics (cf. their experiments 1B and 3B), the rectification process is strong enough to have a significant feed-back on the wave. This can be deduced from the wave amplitude of the linearized experiment, which is smaller by a factor of 2. There is a significant amount of vorticity ς in the time-mean Taylor cap, exceeding $-f$ at the top. We are in a regime where the existing mean flow reduces the ambient vorticity $f + \varsigma$ for the wave in a shallow layer above the seamount and thereby leads to an increased wave response.

The weak residual time-mean flow for the linearized dynamics can be attributed to the weak remaining trend in the forcing and the remnants of transients from the initialization process.

Finally, it should be noted that removing the stratification results in much weaker point-wise velocities; the barotropic response, however, is enhanced.

Resolution Dependence

The issue of horizontal resolution and its influence on the modeling of seamount trapped waves was previously investigated in a more technical paper by Beckmann and Haidvogel (1993). It is obvious that the spatial scales set by the seamount need to be resolved properly, but how stringent are these constraints?

The combination of the terrain-following model concept and the stretched vertical coordinate gives an exceptionally good vertical resolution of the wave and mean flow fields. It is unknown, however, how much horizontal resolution is needed for convergence of the solution and whether there is significant degradation of the result for less resolution. For this reason, a first series of experiments varies the horizontal resolution without changing any other model parameter: identical dissipation and time step are used for all five experiments.

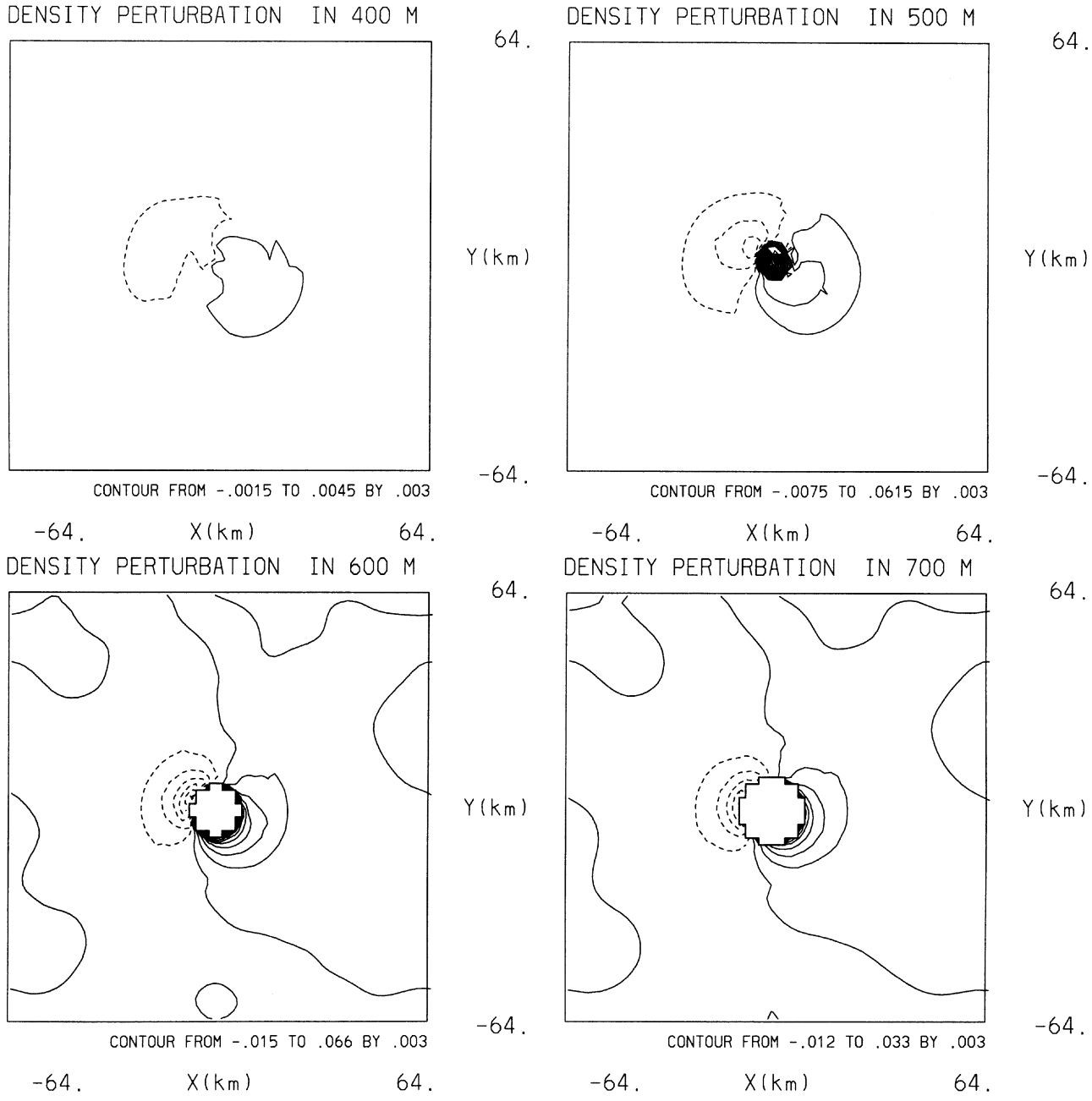

Figure 2. Snapshot of the horizontal structure of the density perturbation for seamount trapped wave in the central experiment: (a) 400 m; (b) 500 m; (c) 600 m; and (d) 700 m. Only the inner quarter of the domain is shown.

Figure 4 summarizes the results: while the wave response and mean flow generation increase with increasing resolution down to about 2 km grid spacing, further increase results in slightly reduced wave amplitudes; the rectified flow seems to have reached convergence.

An explanation involves the fact that the rectification process requires a finite amount of friction to break the symmetry of the seamount trapped wave. Too much friction, however, will damp the wave and reduce the rectified flow. The non-uniform convergence is an indication that the implicit diffusion/viscosity in the numerical model still dominates over the explicitly prescribed values for 4, 3 and 2 km resolution but is below that level for 1.5 and 1 km resolutions.

It should be noted that the results for the least resolving case differ from all others by the apparent existence of a higher vertical mode, a circulation pattern which might be used as evidence for insufficient numerical resolution.

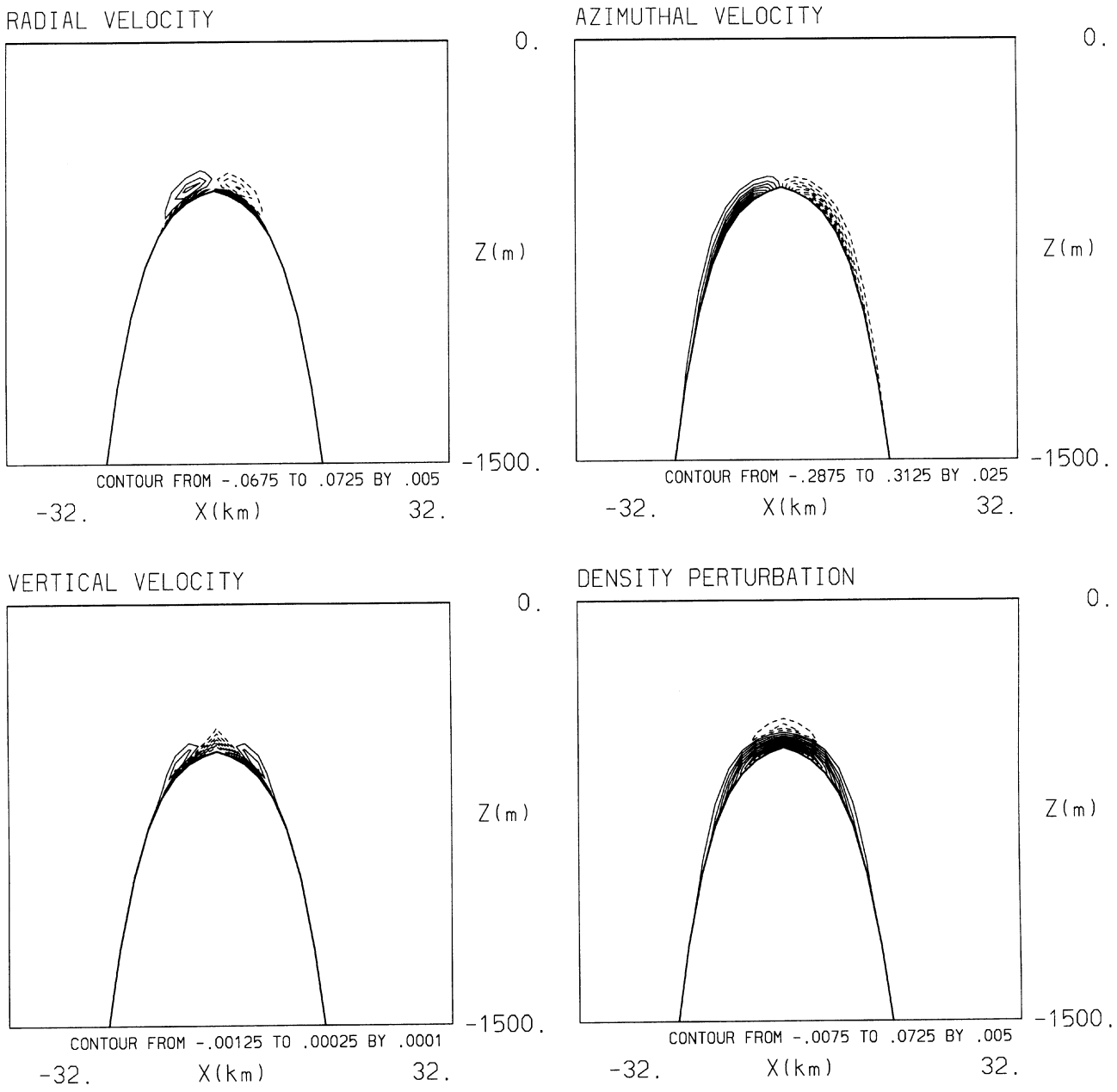

Figure 3. Spatial structure of the time-mean flow in the central experiment: (a) radial velocity; (b) azimuthal velocity; (c) vertical velocity; and (d) density perturbation. Shown is the radial-vertical plane focussing on the upper 1500 m of the inner quarter of the model domain.

Variations of Shape and Topographic Irregularities

While changes of the fractional seamount height and functional form had been considered in previous studies (e.g., Chapman and Haidvogel, 1992), there is no systematic investigation of seamount radius and slope, azimuthal asymmetries and small-scale bottom roughness.

Examples from these three categories of topographic variations are considered in this study. The basic form of the topographic obstacle (2) was modified in the following way:

$$R_o = R_1 + R_2 \sin(n \cdot \theta + \theta_o) \qquad (6)$$

Radial Shape of the Seamount

In this class of variations, the influence of seamount diameter and slope is investigated. The radius of the seamount (R_1) was varied between 15 and 25 km (Fig. 5). The maximum resonance was found for a radius of 20 km, this is for a Burger number of $S = r_D / R_o = 0.5$, which coincides with the central case reported in the previous section.

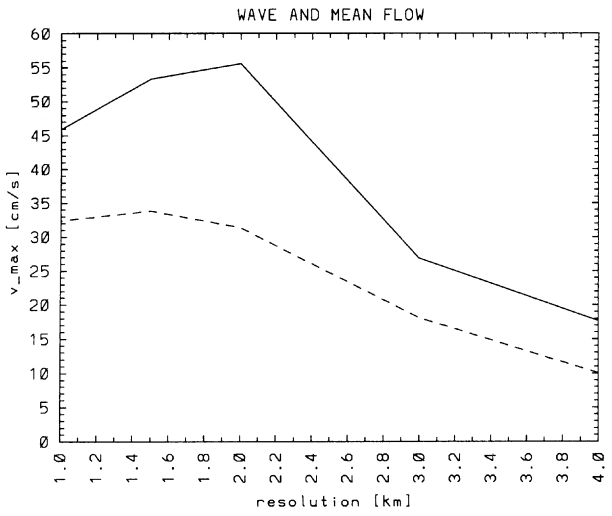

Figure 4. Wave amplification (solid line) and mean flow rectification (dashed line) as a function of horizontal resolution: the maximum point-wise velocity.

The rectified mean flow is directly proportional to the wave amplitude for most of the parameter space, except for very wide seamounts, where the lobes of the seamount trapped wave are separated and cannot interact effectively. Very thin seamounts, on the other hand, seem to have a smaller perturbing effect on the barotropic tidal flow, thus resulting in generally weaker resonance.

In a next step, the slope of the seamount (R_2) was varied between 6 and 12 km (Fig. 6). This represents a change in maximum slope from 16.7 to 33.3%. Again, there is a maximum, in this case at around 9 km, where maximum resonance occurs. Steeper slopes suppress the wave amplitude and essentially eliminate the mean flow generation.

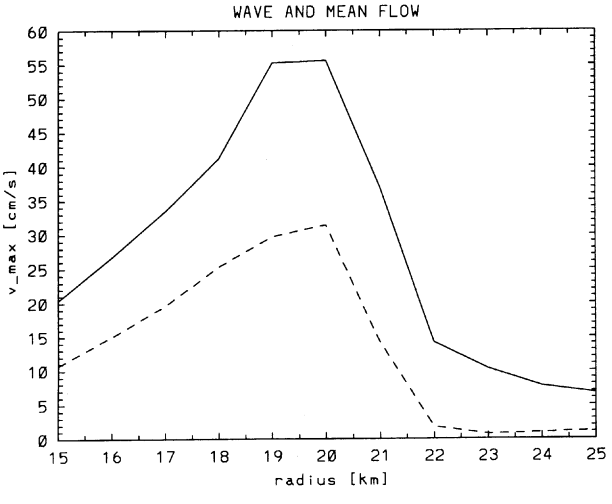

Figure 5. As Fig. 4, but as a function of seamount radius R_1.

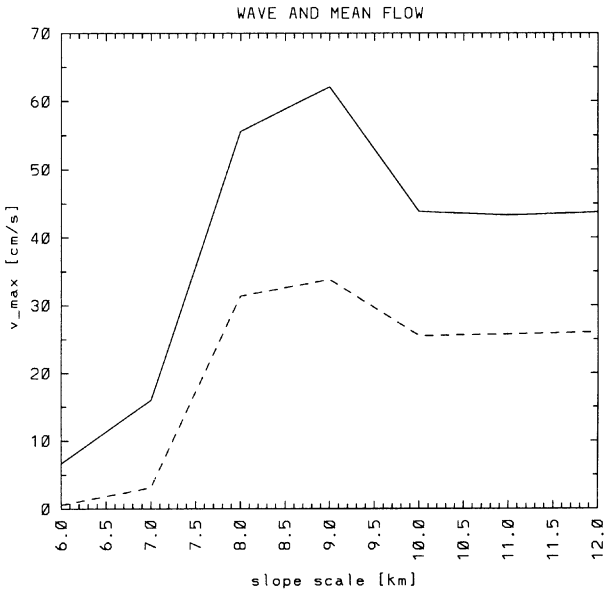

Figure 6. As Fig. 4, but as a function of seamount slope R_2.

Azimuthal Asymmetries

Variations in the azimuthal direction were added in the form of sinusoidal changes in radius of varying mode number. A first series of experiments investigates the effect of amplitude changes for mode 2 asymmetries; subsequently, higher order perturbations were investigated and possible effects of the angle of attack for an asymmetric seamount were tested.

The introduction of an azimuthal asymmetry with $n = 2$ generally reduces the wave and mean flow response (Fig. 7). Obviously, a symmetric seamount has to be regarded

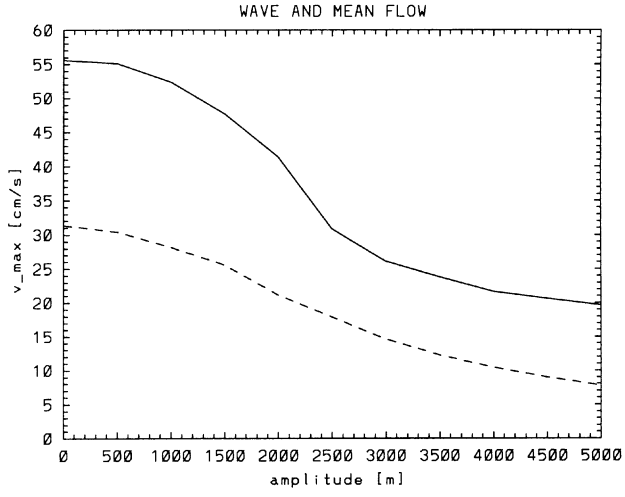

Figure 7. As Fig. 4, but as a function of the amplitude of the mode 2 asymmetry.

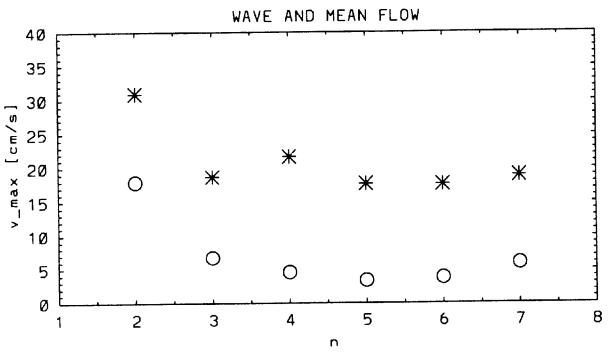

Figure 8. As Fig. 4, but as a function of azimuthal mode number n. Solutions exist only at discrete points: asterisks denote the wave amplification, circles the mean flow rectification.

as the optimal geometry for resonant amplification and rectification. Azimuthal pressure variations of the wave correlated with the topographic asymmetries do not contribute enough to compensate the reduction of wave amplification due to the geometrical changes.

Higher order azimuthal variations (Fig. 8) tend to decorrelate the non-linear interaction between the wave lobes even more. The rectification efficiency drops from 50% to less than 25%.

The orientation of the asymmetric seamount with respect to the main axis of the forcing was varied between θ_o = 0° and 180° (Fig. 9). This "angle of attack" was found to be of only minor importance for the trapped flow response: 10% difference in the wave amplitude is found, with a maximum at θ_o = 0° , when the mean flow hits the obstacle on the larger flanks in prograde direction.

Bottom Roughness

Lastly, the smooth seamount topography was modified by adding a random bottom roughness of varying rms-value. The random perturbations are weighted by the

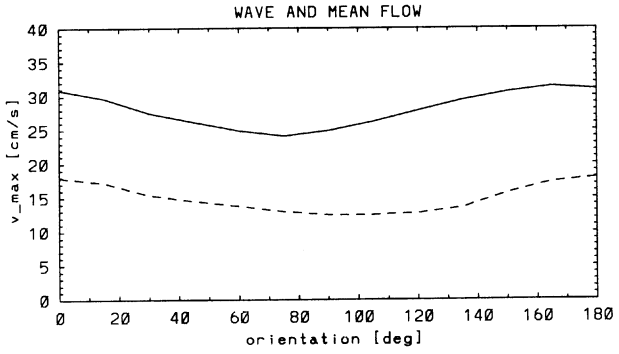

Figure 9. As Fig. 4, but as a function of seamount orientation θ_o relative to the forcing flow.

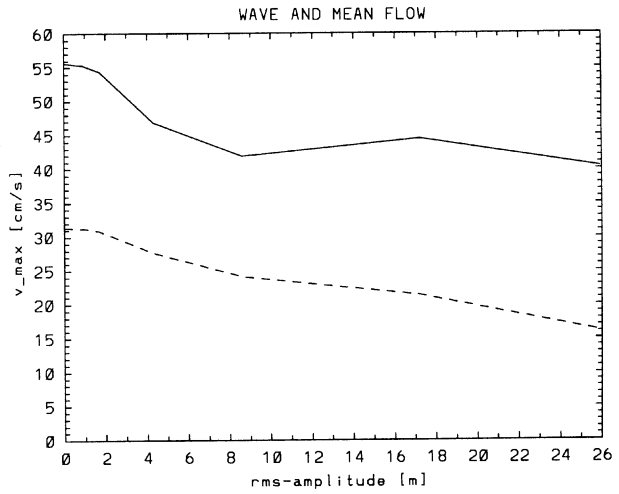

Figure 10. As Fig. 4, but as a function of rms-amplitude of the random bottom roughness.

deviation from maximum water depth, thus being largest on top of the seamount and essentially zero in the deep ocean away from the obstacle. This way, even relatively small rms-values should have an influence on the resonant and rectified flow. The general tendency of added bottom roughness is to act as a sink of wave energy (Fig. 10). Similar to the azimuthal asymmetries, bottom roughness destroys the systematic non-linear interaction of the wave and thus reduces both the amplification and rectification.

Latitudinal Dependence

In addition to the changes in seamount geometry the Coriolis parameter f was varied between 30°N and 65°N to obtain an idea of the sensitivity to environmental parameters.

The dependence on latitude was found to be immense: Figure 11 covers the latitudinal range between 30°N, the critical latitude for trapped diurnal waves, and 65°N and shows large differences in the maximum point-wise velocities across the parameter range. As expected from the studies of Haidvogel et al. (1993), a larger Coriolis parameter (reducing the Burger number) gives much larger response at high latitudes. It is noteworthy, though, that a variation of f by a factor smaller than 2 can account for a change in amplification by a factor of 6.

Implications for Parametrizations

Arguments from statistical mechanics can be used to derive a simplified form of the systematic flow along topographic depth contours caused by interaction between fluctuating flow and topographic variations. A parametrization of this "fifth force" for coarse resolution models was proposed by Holloway (1992): the lateral viscous terms should be modified to drive the barotropic part of the horizontal flow field towards a state of cyclonic

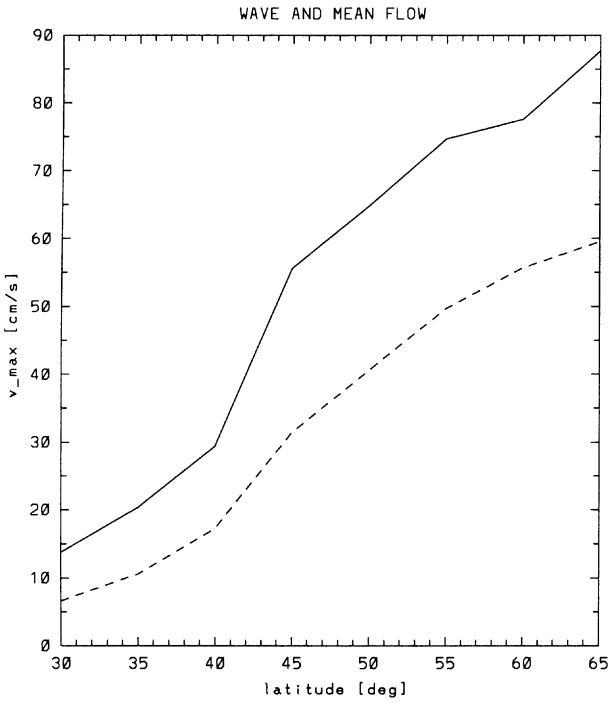

Figure 11. As Fig. 4, but as a function of latitude.

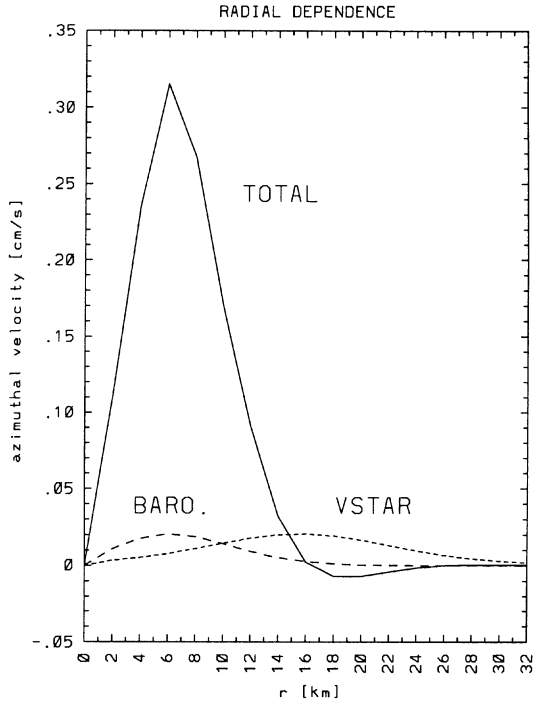

Figure 12. Azimuthal time-mean velocities as a function of radial distance from the seamount center: total bottom flow, barotropic part, and the climatological velocity from eq. (8) with $L = 1200$ m.

circulation around ocean basins. It was shown that this approach can give results closer to observations (Eby and Holloway, 1994).

In principle, the time-mean flow around a seamount is based on the same physical process. It is therefore obvious to ask whether we can learn from these experiments about the structure of mean flows and how to parameterize them?

According to Holloway (1992) the barotropic time-mean "climatological" velocities can be derived from a streamfunction of the form

$$\psi^* = -L^2 fH \tag{7}$$

As a result, the azimuthal component of the mean flow would be approximated by

$$V^* = \frac{1}{H}\psi_r^* = -fL^2\frac{H_r}{H} \tag{8}$$

Figure 12 compares the azimuthal time-mean flow at the bottom and its barotropic part from the central experiment with the V^* from theory.

First of all it is obvious that the barotropic part represents only a small portion of the flow field; the rectified response is mainly baroclinic. But even a look at the barotropic component shows significant differences: while V^* has its maximum at the location of the maximum H_r / H, the model concentrates its time-mean momentum at a smaller radius. As a consequence, maximum velocities and transports do not match. If $L = 1200$ m is chosen (as for Fig. 12), the velocities are comparable, but the transport is too large by a factor of 4. If this is compensated by the choice of a smaller L, the resulting velocities are too small.

It is not clear whether or not we should expect the mean flow structure at seamounts to be fundamentally different from the form stress rectified flow at straight continental slopes, due to the geometric peculiarity of the radially symmetric topography. Further detailed studies are needed.

Similarly, attempts to introduce vertical structure in the parametrization need more attention; they would have to take into account a corresponding density perturbation

$$f v_z^* = -g\rho_r^* \tag{9}$$

but this extension is not straightforward.

Summary and Conclusions

Geometrical and environmental parameters are varied in a series of numerical experiments featuring a tall, steep and isolated seamount forced by diurnal barotropic flow. Several classes of topographic changes and irregularities are investigated for their influence on wave amplification and mean flow generation. Changes of the radial shape of the seamount are found to be the most crucial in determining the actual amplitude of the trapped flow. All azimuthal irregularities tend to reduce the wave response and the amount of rectification.

The results of Haidvogel et al. (1993) are found to be robust through the parameter space. The instantaneous near seamount response is dominated by the first azimuthal mode seamount trapped wave; higher modes could not be detected. However, a regime was found in which the vorticity of the mean flow modified the local environment of the wave enough to cause an enhancement of the wave amplitude through non-linear feed-back.

Returning to the comparison of the real Fieberling Guyot topography and its smooth Gaussian fit we have to conclude that the slightly increased flow amplitudes for the real Fieberling Guyot bathymetry are likely to be the joint effect of steeper slopes that increase and asymmetries combined with bottom roughness that decrease the response.

References

Beckmann, A. and D.B. Haidvogel, 1993: Numerical simulation of flow around a tall isolated seamount. Part I: Problem formulation and model accuracy. *J. Phys. Oceanog.* 23 , 1736–1753.

Beckmann, A. and D.B. Haidvogel, 1994: Resonant Generation of Waves and Mean Currents at Fieberling Guyot. Ocean Sciences Meeting 1994, San Diego, CA.

Brink, K.H., 1989: The effect of stratification on seamount-trapped waves, *Deep-Sea Res.* 36 , 825–844.

Brink, K.H., 1995: Tidal and Lower Frequency Currents Above Fieberling Guyot, *J. Geophys. Res.*, 100, 10,817–10,832.

Chapman, D.C. and D.B. Haidvogel, 1992: Formation of Taylor Caps over a tall, isolated seamount in a stratified ocean. *Geophys. Astrophys. Fluid Dyn.* 64 , 31–65.

Chapman, D.C. and D.B. Haidvogel, 1993: Generation of internal lee waves trapped over a tall isolated seamount. *Geophys. Astrophys. Fluid Dyn.* 69 , 31–65.

Codiga, D.L., 1993: Laboratory realizations of stratified seamount-trapped waves. *J. Phys. Oceanog.* 23 , 2053–2071.

Eby, M. and G. Holloway, 1994: Sensitivity of a large-scale ocean model to a parameterization of topographic stress. *J. Phys. Oceanog.* 24 , 2577–2588.

Eriksen, C.C., 1991: Observations of amplified flows atop a large seamount. *J. Geophys. Res.* 96 , 15227–15236.

Fennel, W., and M. Schmidt, 1991: Responses to topographical forcing. *J. Fluid Mech.* 223 , 209–240.

Haidvogel, D.B., J.L. Wilkin and R.E. Young, 1991: A semi-spectral primitive equation ocean circulation model using vertical sigma and orthogonal curvilinear horizontal coordinates. *J. Comp. Phys.* 94 , 151–185.

Haidvogel, D.B., A. Beckmann, D.C. Chapman and R.-Q. Lin, 1993: Numerical Simulation of Flow Around a Tall Isolated Seamount: Part II: Resonant Generation of Trapped Waves. *J. Phys. Oceanog.* 23 , 2373–2391.

Haidvogel, D.B. and K.H. Brink, 1986: Mean currents driven by topographic drag over the continental shelf and slope. *J. Phys. Oceanog.* 16 , 2159–2171.

Hogg, N.G., 1980: Effects of bottom topography on ocean currents. In: Orographic Effects in Planetary Flows, *GARP Publication Series*, 23, 167–205.

Holloway, G., 1992: Representing topographic stress for large-scale ocean models. *J. Phys. Oceanog.* 22, 1033–1046.

Holloway, G., K. Brink and D. Haidvogel, 1989: Topographic stress in coastal circulation dynamics. In: Neshyba, S., et al. (eds.), *Poleward Flows along Eastern Ocean Boundaries.* Coastal and Estuarine Studies, 34, Springer-Verlag, New York, 374 pp.

McCalpin, J.D., 1994: A comparison of second-order and fourth-order pressure gradient algorithms in a σ-ordinate ocean model. *Int. J. Num. Meth. Fl.*, 18, 361–383.